Optics Letters

Q-factor and absorption enhancement for plasmonic anisotropic nanoparticles

Wei Liu,[1,2,*] Bing Lei,[1] and Andrey E. Miroshnichenko[2]

[1]College of Optoelectronic Science and Engineering, National University of Defense Technology, Changsha, China
[2]Nonlinear Physics Centre, Australian National University, Acton ACT 0200, Australia
*Corresponding author: wei.liu.pku@gmail.com

Received 16 June 2016; revised 3 July 2016; accepted 3 July 2016; posted 7 July 2016 (Doc. ID 268518); published 26 July 2016

We investigate the scattering and absorption properties of anisotropic metal–dielectric core–shell nanoparticles. It is revealed that the radially anisotropic dielectric layer can accelerate the evanescent decay of the localized resonant surface modes, leading to *Q*-factor and absorption rate enhancement. Moreover, the absorption cross section can be maximized to reach the single resonance absorption limit. We further show that such artificial anisotropic cladding materials can be realized by isotropic layered structures, which may inspire many applications based on scattering and absorption of plasmonic nanoparticles.

OCIS codes: (290.5850) Scattering, particles; (240.6680) Surface plasmons; (160.1190) Anisotropic optical materials.

http://dx.doi.org/10.1364/OL.41.003563

In the field of nanophotonics and many other interdisciplinary subjects, optical waveguides and resonators play an essential role, which provide an indispensable platform for efficient light–matter interactions [1]. Behind different sorts of waveguides and resonators, there are various mechanisms for spatial confinement of light at different scales, of which the total internal reflection (TIR) is probably the most widely employed principle. Nevertheless, many applications (such as high-precision sensing and nanoscale lasing) pose more stringent requirements of stronger electromagnetic localization that convectional TIR-based optical devices can barely meet. Recently a modified version of TIR has been introduced (the so-called relaxed total internal reflection, RTIR), which shows that at the interface of anisotropic and isotropic dielectrics, evanescent waves could decay much faster [2]. Based on such a more general principle of TIR, stronger electromagnetic field confinement has been demonstrated in both optical waveguides [2] and resonators [3], which directly leads to all-dielectric waveguiding beyond the diffraction limit and low-order resonances of significantly higher *Q*-factors.

Besides TIR, electromagnetic surface waves [4,5] provide an alternative significant approach for photonic energy confinement, of which the subject of surface plasmon waveguides and resonators stands as currently the most outstanding example [6]. For many applications based on plasmonic structures, such as nanoscale lasing [7,8], sensing [9], and photovoltaic devices [10], efficient manipulation of scattering and absorption for plasmonic resonances is required, which usually involves special structure design and geometric tuning [11–16].

In this Letter, inspired by the principle of RTIR, the effects of anisotropic dielectric layers on the localized surface plasmonic resonances are studied. It is demonstrated that the anisotropy can effectively provide an additional degree of freedom for manipulation of scattering and absorption cross sections. More specifically, we investigate the scattering of a core (metal)-shell (radially anisotropic dielectric) nanowire and show that the dielectric anisotropy accelerates the decay of the plasmonic mode at the metal–dielectric interface, leading to higher *Q*-factors of the plasmonic resonances. It is further revealed that, due to stronger light confinement effect induced by the anisotropic layer, the resonance absorption can be maximized to reach the single resonance absorption limit with properly designed resonators. We expect that the mechanism we have proposed can shed new light not only on many plasmonic structure-based applications, such as nanolasing, sensing, and photovoltaic devices, but also on the investigations into scattering properties of two-dimensional (2D) structures that are intrinsically highly anisotropic [17].

In Fig. 1(a) we show schematically the nonmagnetic ($\mu = 1$) core–shell structure under consideration: the isotropic metallic

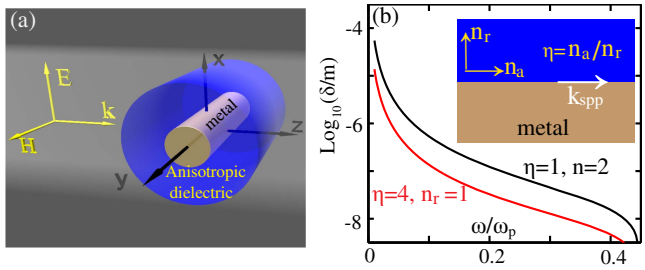

Fig. 1. (a) Schematic illustration of the scattering of a normally incident TM-polarized plane wave by a metal core–dielectric shell nanowire. The radii for the core and shell layers are R_1 and R_2, respectively, and the dielectric layer is radially anisotropic on the x–z plane of azimuthal and radial indices n_a and n_r, respectively. (b) The change of decay length with frequency for the plasmonic mode at the semi-infinite metal-anisotropic dielectric interface (inset). The indices of the dielectric layer are n_a and n_r along the propagating and perpendicular directions, respectively. The anisotropy parameter is defined as $\eta = n_a/n_r$.

core of radius R_1 with permittivity ϵ_m coated by a radially anisotropic dielectric layer of radius R_2. On the x–z plane the radial and azimuthal refractive indices are n_r and n_a, respectively, and the anisotropy parameter is defined as $\eta = n_a/n_r$; the normally incident plane wave is of transverse magnetic (TM) polarization (the magnetic field is fixed along the y direction, axis of the nanowire) to ensure the excitation of the plasmonic modes. We note here that for the transverse electric polarization, as there is only one electric field component along the y direction and thus the mode is not affected by the radial anisotropy on the x–z plane.

To understand the effects of the anisotropic layer on the plasmonic-type resonances, we start with the fundamental waveguiding structure of semi-infinite metal-anisotropic dielectric configuration [shown as the inset of Fig. 1(b)]: the dielectric indices along the propagating and perpendicular directions are set to be n_a and n_r, respectively [consistent with the dielectric layer in Fig. 1(a)]. The angular wavenumber of the supported TM plasmonic mode is [4]

$$k_{\mathrm{spp}} = k\sqrt{\frac{\epsilon_m\epsilon_d(\epsilon_d-\epsilon_m)}{\epsilon_d^2-\eta^2\epsilon_m^2}}, \tag{1}$$

where k is the angular wavenumber in the background material (vacuum in this study) and $\epsilon_d = n_a^2$. As a result, the angular wavenumber along the perpendicular direction in the dielectric layer can be expressed as [1,2]

$$k_d^{\perp} = \sqrt{\epsilon_d k^2 - \eta^2 k_{\mathrm{spp}}^2}. \tag{2}$$

Then we define the perpendicular decay length of the plasmonic mode in the dielectric layer as

$$\delta = \mathrm{Im}(k_d^{\perp})^{-1}, \tag{3}$$

where $\mathrm{Im}(\cdot)$ corresponds to the imaginary part. To demonstrate how the anisotropic dielectric layer accelerates the evanescent decay of the plasmonic mode, in Fig. 1(b) we show the decay length for both isotropic and anisotropic cases: the refractive index of isotropic dielectric layer is fixed at $n = 2$ and for better comparison the indices of the anisotropic dielectric layer are restricted by $n_a n_r = n^2$, and as a result $\eta = (n_a/n)^2$ (as is the case throughout this Letter). Without loss of generality, we employ the Drude model for the metal $\epsilon_m = 1 - \omega_p^2/\omega^2$, where ω is the angular frequency and ω_p is the bulk plasmon frequency. It is clear from Fig. 1(b) that for the anisotropic case, the decay length is much smaller, indicating much faster exponential decay along the perpendicular direction.

According to the correspondence between localized and propagating surface plasmons [16], similar to the demonstration of Q-factor enhancement for RTIR-based all-dielectric resonators [3], we expect that the anisotropic dielectric layer can also improve the Q-factor of plasmonic resonances. To justify this point, now we study directly the scattering properties of the configuration shown in Fig. 1(a). This seminal 2D scattering problem has been well studied [3,18,19], and the scattering and absorption cross sections can be expressed, respectively, as

$$C_{\mathrm{sca}} = \frac{4}{k}\left(|a_0|^2 + 2\sum_{m=1}^{\infty}|a_m|^2\right),$$
$$C_{\mathrm{abs}} = \frac{4}{k}\left[\Upsilon(a_0) + 2\sum_{m=1}^{\infty}\Upsilon(a_m)\right], \tag{4}$$

where the function $\Upsilon(x)$ is defined as $\Upsilon(x) = \mathrm{Re}(x) - |x|^2$, and $\mathrm{Re}(\cdot)$ means the real part; a_0 and a_m are the scattering coefficients, which are η dependent. Then the scattering and absorption efficiencies are $Q_{\mathrm{sca,abs}} = C_{\mathrm{sca,abs}}/2R_2$. Here in this work we confine our study to the plasmonic mode of the lowest order (electric dipole, ED), which corresponds to the scattering coefficient a_1 [20,21] and it is actually quite natural to extend such study to other higher-order plasmon resonances of TM nature.

In Fig. 2(a) we show the scattering and absorption efficiencies (the total efficiency and that contributed by ED only) for the nanowire of $R_1 = 150$ and $R_2 = 350$ nm for both the isotropic case of $\eta = 1$ and the anisotropic case of $\eta = 4$. The metal is gold with the permittivity taken from experimental data [22]. It is clear that the anisotropic cladding makes the ED resonance sharper, indicating a higher Q-factor. To clarify the origin we choose the two scattering resonant positions indicated in Fig. 2(a) ($\lambda_D = 1.5$ μm and $\lambda_{D'} = 1.28$ μm), and the corresponding near-field distributions ($|H_y|^2$) at those two points are shown in Figs. 2(b) and 2(c), respectively. As is the case for the anisotropic metal–dielectric waveguide [shown in Fig. 1(b)], the sharper resonance is induced by the tighter localization of the plasmonic mode at the interface along the radial direction [see Figs. 2(b) and 2(c)], which enables stronger electromagnetic energy confinement. To give more details concerning how the Q-factor of the resonance is affected by η, in Fig. 2(d) we show specifically its dependence, where the Q-factor is approximated by fitting the scattering curves into a Lorentzian distribution [1,3]. It is quite clear that the anisotropic dielectric layer can effectively enhance the Q-factor of the plasmonic resonances.

In addition to the Q-factor improvements, the results in Fig. 2(a) also demonstrate the enhancement of the absorption

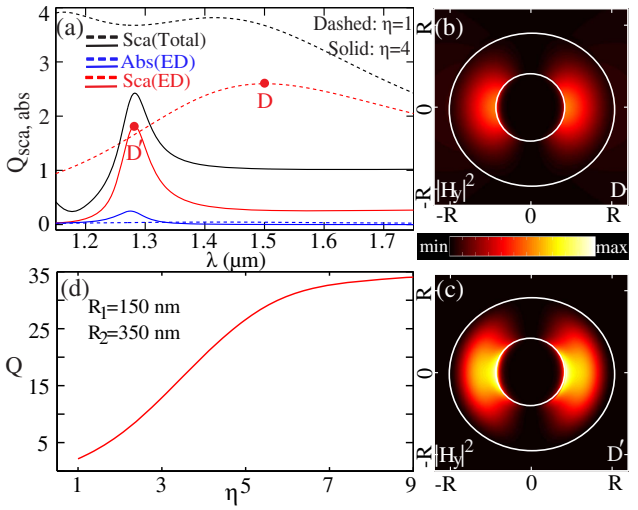

Fig. 2. (a) Scattering (red curves) and absorption (blue curves) efficiency spectra (both total efficiency and that of the ED) for the core–shell nanowire of $R_1 = 150$ nm and $R_2 = 350$ nm. The results for both the isotropic ($\eta = 1$, dashed curves) and anisotropic ($\eta = 4$, solid curves) cases are shown. The scattering resonant positions of ED are denoted by D and D', respectively ($\lambda_D = 1.5$ μm and $\lambda_{D'} = 1.28$ μm), and the corresponding near-field distributions (in terms of $|H_y|^2$) are shown in (b) and (c). (d) The dependence of the Q-factor of the ED resonance on the anisotropy parameter.

at the resonance (see blue curves). As a next step, we study in detail how the anisotropy can be employed for the maximization of the plasmonic resonance absorption [23,24]. For the 2D scattering configuration shown in Fig. 1(a), it is known that there exists a single channel absorption cross-section limit [14,16,25–27]:

$$C_{\mathrm{lim}} = \frac{\lambda}{4\pi}, \tag{5}$$

which can be reached if at the resonant position the scattering and absorption rates are equal to each other [16,27–29]. Despite the magnetic dipole resonance (characterized by a_0), all other resonances including ED actually correspond to two degenerate channels [20,21], of which the absorption limit is consequently $2C_{\mathrm{lim}}$. In Fig. 3(a) we show the normalized ED absorption cross sections $N_{\mathrm{abs}} = C_{\mathrm{abs}}/2C_{\mathrm{lim}}$ for the core–shell nanowire of $R_1 = 75$ and $R_2 = 150$ nm. Four cases are investigated for $\eta = 1, 3, 4, 5$. It is clear that in the spectrum region shown, the absorption has been significantly enhanced when the anisotropic shell is introduced. For the three anisotropic cases the absorption resonant positions are indicated, where at P_1 of $\eta = 4$ the single resonance absorption limit is reached. For this special case, we also show in Fig. 3(a) the normalized ED scattering spectra $N_{\mathrm{sca}} = C_{\mathrm{sca}}/2C_{\mathrm{lim}}$. It is clear that at P_1 the scattering and absorption rates (cross sections) are equal, which leads to the absorption maximization. At the other two points P_2 ($\eta = 5$) and P_3 ($\eta = 3$), the scattering rates are smaller and larger, respectively, than the absorption rates, leaving the single resonance absorption limit untouched. Moreover, a proper geometric tuning and selection of the anisotropy parameters can help to achieve the optimal absorption at various resonant frequencies. In Fig. 3(b) we show three cases with fixed shell layer width of $R_2 = 150$ nm while with different combinations of core radii and anisotropy parameters, when the absorption reaches the maximum value at different wavelengths. We note that here we demonstrate the absorption maximization in the visible spectral region where the loss of Au is relatively high. Such enhancement can certainly be achieved at other spectrum regions of lower intrinsic loss rate, where, however, larger anisotropy parameters are required.

Finally, we discuss the possible realizations of the scattering resonators discussed above. For natural materials, the anisotropy parameters are usually low and thus would not significantly affect the Q-factor or the absorption of the low-order plasmonic resonances. Nevertheless, with the recent rapid progress in the field of metamaterials, many exotic features of materials, including unusual refractive indices and anisotropy parameters have been obtained [30–32]. To achieve large anisotropy parameters of the dielectric layer, we employ a multilayered cladding consisting of two isotropic dielectrics of positive refractive indices n_1 and n_2 [$n_1 < n_2$, see Fig. 4(a)]. As long as each dielectric layer width is far smaller than the effective wavelength in the layers, the effective medium theory can be applied [3,31], and then the effective indices for the multilayered cladding along the radial and azimuthal directions are, respectively,

$$n_{\mathrm{r}} = n_1 n_2 / \sqrt{(1-f)n_1^2 + f n_2^2},$$
$$n_{\mathrm{a}} = \sqrt{f n_1^2 + (1-f) n_2^2}, \tag{6}$$

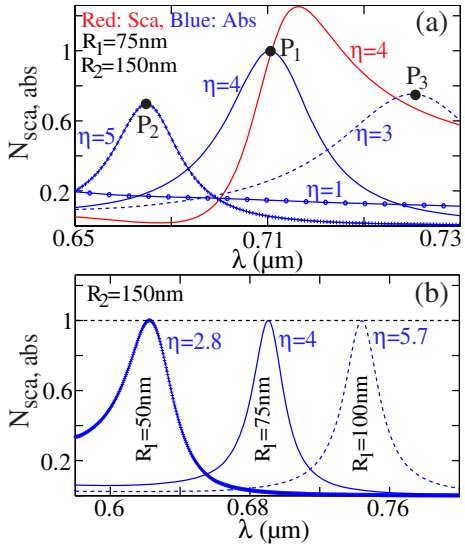

Fig. 3. (a) Normalized absorption cross-section spectra (blue curves) for the core–shell nanowire of $R_1 = 75$ and $R_2 = 150$ nm. Four cases of $\eta = 1, 3, 4, 5$ are studied and the absorption resonant positions for the anisotropic cases of $\eta \neq 1$ are indicated by $P_{1,2,3}$. For $\eta = 4$ when the single resonance absorption limit can be reached, the normalized scattering cross-section spectrum (red curve) is also shown. (b) Normalized absorption cross-section spectra for core–shell nanowires of fixed shell radius of $R_2 = 150$ nm. Three combinations of core radius and anisotropy parameter are shown, where the absorption has been maximized at different resonant positions.

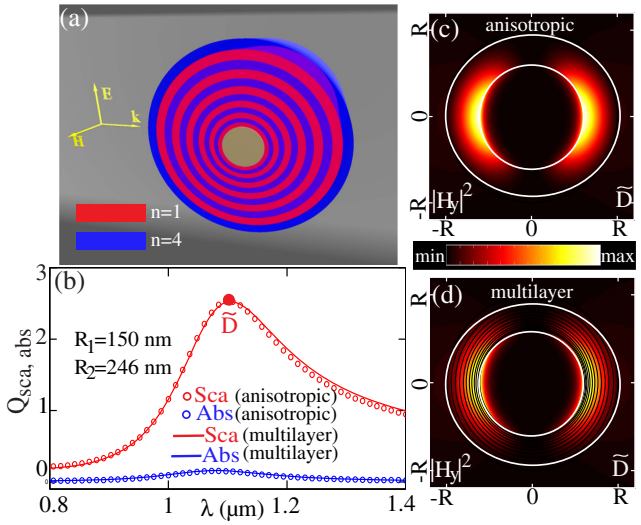

Fig. 4. (a) The schematic of the scattering configuration where a relatively large effective anisotropy parameter can be obtained for the cladding layer: the metallic core $R_1 = 150$ nm is surrounded by alternating isotropic dielectric layers of indices of n_1 and n_2 with linearly increasing layer widths ($R_2 = 246$ nm). The corresponding scattering and absorption efficiency spectra are shown in (b) by solid curves, where the spectra for the corresponding two-layered metal-anisotropic dielectric nanowire of $n_a = 2.92$, $n_r = 1.37$ are also shown by circles for comparison. The resonant position of $\lambda = 1.1$ μm is indicated and at this position the near-field distributions (in terms of $|H_y|^2$) are shown for both cases in (c) and (d).

where f is the filling factor of the higher-index layer in terms of layer width. As a result, the radial anisotropy parameter obtained is

$$\eta(f) = \frac{\sqrt{f n_1^2 + (1-f) n_2^2}\sqrt{(1-f) n_1^2 + f n_2^2}}{n_1 n_2}. \quad (7)$$

The highest anisotropy parameter obtainable is $\eta_{\max} = (n_1^2 + n_2^2)/2n_1 n_2$ when $f = 0.5$. To be consistent with the index parameters adopted already in this work, we study the simple case of $n_1 = 1$ and $n_2 = 4$, which makes effectively $n_a n_r = n^2 = 4$ ($n_a = 2.92$, $n_r = 1.37$) and $\eta_{\max} = 2.13$ when $f = 0.5$. To achieve $\eta_{\max}$, as long as the effective medium theory can be applied and $f = 0.5$, the specific layer width is not important and thus of course the whole cladding does not have to be periodic. We give a simple example here: the metal core ($R_1 = 150$ nm) is covered by six dielectric unit cells and each unit cell is made of two dielectric layers with different indices but the same width (this makes $f = 0.5$); each layer width in the i-th unit cell is $d_i = (2i + 1)$ nm for $i = 1{:}6$ [see the schematic shown in Fig. 4(a)] and consequently $R_2 = 246$ nm. The scattering and absorption efficiency spectra of such an isotropic multilayered resonator are shown in Fig. 4(b) (solid curves), which agree very well with the results (shown in circles) of the corresponding two-layered metal-anisotropic dielectric nanowire of $n_a = 2.92$ and $n_r = 1.37$. Furthermore, we show also the near-field distributions of $|H_y|^2$ at the scattering resonant position [indicated by $\tilde{D}$ in Fig. 4(b) and $\lambda_{\tilde{D}} = 1.1$ μm] in Figs. 4(c) and 4(d) for both cases, which also agree quite well. Those results can justify the effectiveness of our approach for resonance control relying on dielectric anisotropy.

To conclude, we propose and demonstrate the efficient engineering of Q-factor and absorption for plasmonic resonances relaying an anisotropic cladding layer. By analyzing the scattering properties of the anisotropic core–shell metal–dielectric nanowires, we reveal that the resonance Q-factor can be enhanced and the absorption can be maximized to reach the ultimate single resonance limit due to the faster evanescent decay and thus stronger energy confinement of the localized surface plasmonic modes. We note that the principle we have revealed can certainly be applied to higher-order modes and resonators of other shapes, and also to other anisotropy, such as permeability anisotropy, and to other sorts of surface modes [5]. For the proof-of-concept demonstration, we adopt a multilayered lossless cladding that exhibits moderate effective anisotropy parameter ($\eta_{\max} = 2.13$). Nevertheless, we have to keep in mind that relying on metamaterials and 2D materials, much more exotic anisotropy features can be obtained (including complex anisotropy parameters) [17,30–32]. This may enable much stronger field localization and more flexible resonance manipulations, thus shedding new light on many plasmonic metamaterials and 2D materials-based fundamental research and applications.

Funding. National Natural Science Foundation of China (NSFC) (11404403); Australian Research Council (ARC); Basic Research Scheme of College of Optoelectronic Science and Engineering; National University of Defence Technology (NUDT).

Acknowledgment. We thank D. A. Powell, D. N. Neshev, and Yuri S. Kivshar for useful discussions, and acknowledge the financial support from the National Natural Science Foundation of China (Grant number: 11404403), the Australian Research Council, and the Basic Research Scheme of College of Optoelectronic Science and Engineering, National University of Defense Technology. W. L. thanks the Nonlinear Physics Centre for a warm hospitality during his visit to Canberra.

REFERENCES

1. B. E. A. Saleh and M. C. Teich, *Fundamentals of Photonics* (Wiley, 2013).
2. S. Jahani and Z. Jacob, Optica **1**, 96 (2014).
3. W. Liu, A. E. Miroshnichenko, and Y. S. Kivshar, "Q-factor enhancement in all-dielectric anisotropic nanoresonators," arXiv:1603.02111 (2016).
4. A. D. Boardman, *Electromagnetic Surface Modes* (Wiley, 1982).
5. J. Polo, T. Mackay, and A. Lakhtakia, *Electromagnetic Surface Waves: A Modern Perspective* (Newnes, 2013).
6. S. A. Maier, *Plasmonics: Fundamentals and Applications* (Springer, 2007).
7. R. F. Oulton, V. J. Sorger, T. Zentgraf, R. M. Ma, C. Gladden, L. Dai, G. Bartal, and X. Zhang, Nature **461**, 629 (2009).
8. M. A. Noginov, G. Zhu, A. M. Belgrave, R. Bakker, V. M. Shalaev, E. E. Narimanov, S. Stout, E. Herz, T. Suteewong, and U. Wiesner, Nature **460**, 1110 (2009).
9. A. V. Kabashin, P. Evans, S. Pastkovsky, W. Hendren, G. A. Wurtz, R. Atkinson, R. Pollard, V. A. Podolskiy, and A. V. Zayats, Nat. Mater. **8**, 867 (2009).
10. H. A. Atwater and A. Polman, Nat. Mater. **9**, 865 (2010).
11. E. Feigenbaum and M. Orenstein, Phys. Rev. Lett. **101**, 163902 (2008).
12. B. Min, E. Ostby, V. Sorger, E. Ulin-Avila, L. Yang, X. Zhang, and K. Vahala, Nature **457**, 455 (2009).
13. A. E. Miroshnichenko, S. Flach, and Y. S. Kivshar, Rev. Mod. Phys. **82**, 2257 (2010).
14. Z. C. Ruan and S. H. Fan, Phys. Rev. Lett. **105**, 013901 (2010).
15. B. Luk'yanchuk, N. I. Zheludev, S. A. Maier, N. J. Halas, P. Nordlander, H. Giessen, and C. T. Chong, Nat. Mater. **9**, 707 (2010).
16. W. Liu, R. F. Oulton, and Y. S. Kivshar, Sci. Rep. **5**, 12148 (2015).
17. F. Xia, H. Wang, D. Xiao, M. Dubey, and A. Ramasubramaniam, Nat. Photonics **8**, 899 (2014).
18. M. Kerker, *The Scattering of Light, and Other Electromagnetic Radiation* (Academic, 1969).
19. H. Chen and L. Gao, Phys. Rev. A **86**, 033825 (2012).
20. K. Vynck, D. Felbacq, E. Centeno, A. I. Cabuz, D. Cassagne, and B. Guizal, Phys. Rev. Lett. **102**, 133901 (2009).
21. W. Liu, A. E. Miroshnichenko, R. F. Oulton, D. N. Neshev, O. Hess, and Y. S. Kivshar, Opt. Lett. **38**, 2621 (2013).
22. P. B. Johnson and R. W. Christy, Phys. Rev. B **6**, 4370 (1972).
23. R. A. Depine and M. L. Gigli, Opt. Lett. **20**, 2243 (1995).
24. L.-W. Chou, R. D. Near, D. S. Boyuk, and M. A. Filler, J. Phys. Chem. C **118**, 5494 (2014).
25. T. J. Seok, A. Jamshidi, M. Kim, S. Dhuey, A. Lakhani, H. Choo, P. J. Schuck, S. Cabrini, A. M. Schwartzberg, J. Bokor, E. Yablonovitch, and M. C. Wu, Nano Lett. **11**, 2606 (2011).
26. R. E. Hamam, A. Karalis, J. D. Joannopoulos, and M. Soljacic, Phys. Rev. A **75**, 053801 (2007).
27. A. E. Miroshnichenko and M. I. Tribelsky, "The ultimate absorption at light scattering by a single obstacle," arXiv:1603.03513 (2016).
28. R. Fleury, J. Soric, and A. Alu, Phys. Rev. B **89**, 045122 (2014).
29. S. Tretyakov, Plasmonics **9**, 935 (2014).
30. M. Choi, S. H. Lee, Y. Kim, S. B. Kang, J. Shin, M. H. Kwak, K. Y. Kang, Y. H. Lee, N. Park, and B. Min, Nature **470**, 369 (2011).
31. A. Poddubny, I. Iorsh, P. Belov, and Y. Kivshar, Nat. Photonics **7**, 948 (2013).
32. C. Wu, A. Salandrino, X. Ni, and X. Zhang, Phys. Rev. X **4**, 021015 (2014).